Macromolecules

pubs.acs.org/Macromolecules Article

Facile Synthesis of High-Molecular-Weight Biobased Polythioethers with Outstanding Mechanical Properties and Intrinsic Antiultraviolet Performance

Qiubo Wang, Xinyu Hu, Min Yan, Xingyu Luo, Xiaojuan Liao,* and Meiran Xie*

Cite This: Macromolecules 2025, 58, 4769−4779 Read Online

ACCESS | Metrics & More | Article Recommendations | Supporting Information

ABSTRACT: Common methods, including adding inorganic and organic ultraviolet (UV) absorbers, for preparing anti-UV polymers inevitably have the disadvantages of poor stability, low transparency, and coloration of samples. To overcome these shortcomings, high-molecular-weight polythioethers with excellent intrinsic anti-UV performance were prepared by anion ring-opening polymerization of episulfides derived from the biobased epoxides containing a substituted phenyl group. The mechanical properties, reprocessability, and anti-UV performance of polythioethers were significantly improved through copolymerization and cross-linking modification. A cross-linked copolythioether displayed a UV protection factor value of 91.8 and a light transmittance of over 68% in the visible range and moreover exhibited outstanding mechanical properties with a tensile strength of 17.9 MPa and an elongation at break of 534%. The mechanical properties and anti-UV performance of copolythioether decreased significantly after prolonged exposure to UV light, while the cross-linked copolythioether maintained good stability. This work provided a feasible method for preparing colorless, transparent, and high-performance intrinsic anti-UV polythioethers, which can be used in the manufacture of lenses and can effectively prevent UV-light damage to the eyes.

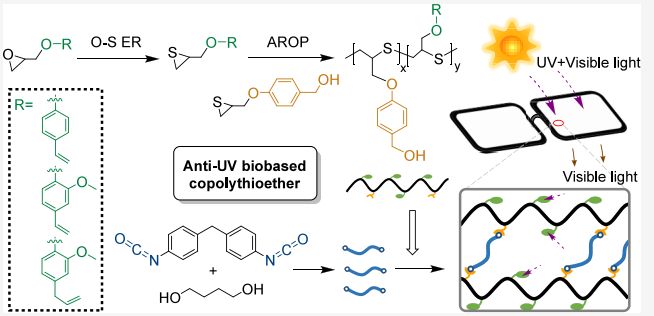

INTRODUCTION

Ultraviolet (UV) in sunlight can be divided into UVA (320−400 nm), UVB (280−320 nm), and UVC (200−280 nm);[1] due to the role of ozone present in the stratosphere, of these, only most of the UVA and a small amount of UVB can reach the Earth's surface.[2] Although the UV radiation in moderation has a bactericidal effect,[3] with the destruction of the environment, the balance of stratospheric ozone is broken, which resulted in an increase in UV radiation. This will not only lead to sunburn,[4] various skin diseases and cancer,[5] but also affect the growth of plants as well as accelerating the aging of polymer materials.[6,7] Therefore, the pursuit of additional UV protection properties has become a major trend in material manufacturing.[8−10] Anti-UV materials can be divided into two parts: a substrate and a UV absorber, between which inorganic and organic absorbers have been widely used as classic UV absorbers.[11,12] However, inorganic UV absorbers have higher absorption capacity in the visible region,[13,14] which reduced the transparency of the material, while organic absorbers have disadvantages such as poor stability or potential toxicity.[2,15,16] In addition, petroleum-based polymers are widely used as substrates for anti-UV materials manufacturing with their extensive source, lower cost, and excellent durability.[17,18] It is urgent to develop sustainable biobased polymers to replace petroleum-based polymers, which have nonrenewable and nondegradable properties, in order to achieve the goal of sustainable development.

Lignin has been considered an ideal alternative to chemical UV absorbers due to its high-level safety and plant-derived properties.[19,20] The functional groups of aryl, phenolic hydroxyl, ketone, and carboxylic groups are present in lignin, together with intramolecular hydrogen bonding and conjugation, of which structural properties endowed lignin with excellent anti-UV properties.[21,22] However, the unmodified lignin particles would degrade the mechanical properties of the polymer films due to poor dispersibility in the matrix.[2] Strong alkaline or acidic conditions and organic solvents can be used in the extraction of lignin, which made the color of the lignin darker, so that it is impossible to produce light-colored lignin.[1] Unfortunately, it is difficult to obtain lignin materials with both excellent anti-UV performance and light color. Selecting suitable lignin derivatives or biomass with a structure similar to the starting monomers of polymers to prepare high-

Received: February 11, 2025
Revised: April 1, 2025
Accepted: April 11, 2025
Published: April 23, 2025

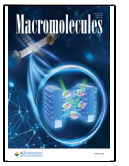

https://doi.org/10.1021/acs.macromol.5c00389
Macromolecules 2025, 58, 4769−4779

performance anti-UV polymers could be a feasible solution. Eugenol (UG) is a natural allyl-substituted guaiacol, which can be extracted from plants rich in clove oil or prepared by catalytic conversion of lignin.[23−25] UG has a unique bifunctional structure (bearing hydroxyl and allyl groups), which could be used as a polymerizable group for modification.[26−28] 4-Vinylphenol and 2-methoxy-4-vinylphenol are biobased derivatives with unique phenol structure and vinyl functional groups, which can be used as polymerizable groups for modification.[29−31] Unfortunately, they have so far been poorly developed in the field of intrinsic anti-UV polymers.

Polythioethers are a kind of functional polymer with unique electrical and photoelectric properties,[32,33] but their preparation by conventional anionic ring-opening polymerization (AROP) of episulfides usually takes place under stringent conditions.[34] The oxygen−sulfur exchange reaction (O−S ER) is becoming more and more widely used in polymer synthesis.[35−37] A previous research combined O−S ER of epoxide with aqueous anionic ring-opening polymerization (AAROP) of the in situ generated episulfide and established a green cascade O−S ER/AAROP approach to prepare structurally controllable polythioethers.[38] The thiocyanate supplied a sulfur source for the O−S ER of epoxide and created a strongly alkaline environment (pH ≈ 12) that enhanced the nucleophilicity of the anion ($^{-}$SCN), which facilitated AAROP of episulfide. Unlike AROP in organic solvents, which usually required a moisture- and oxygen-free environment, the cascade O−S ER/AAROP in water and an open vessel allowed epoxide to form polythioether directly. Yet, polythioethers prepared by this one-pot approach usually have only moderate molecular weight owing to the poor solubility of most episulfides in the water phase, which limited their application. In this work, three biobased epoxides, 2-(4-vinyl phenoxymethyl) epoxide (VPE), 2-(2-methoxy-4-vinyl phenoxymethyl) epoxide (MVPE), and 2-(2-methoxy-4-allyl phenoxymethyl) epoxide (MAPE), were synthesized in consideration of the structural characteristics of biobased derivatives, which were then used to prepare the corresponding episulfides by the O−S ER with thiocyanate. Subsequently, high-molecular-weight biobased polythioethers were obtained by AROP of episulfides in an open vessel and an undried polar solvent. Due to the presence of conjugated side chains and the introduction of sulfur atoms, the prepared polythioethers possessed excellent anti-UV performance. Furthermore, novel anti-UV polymeric materials with enhanced mechanical properties were prepared by a cross-linking reaction of poly(hydroxyl thioether) with a long-chain isocyanate.

EXPERIMENTAL SECTION

Materials. UG (99%), 2-methoxy-4-vinylphenol (98%), 4-vinylphenol (10 wt % in propylene glycol), epichlorohydrin (99%), potassium carbonate (K_2CO_3, 99%), potassium iodide (KI, 99%), potassium thiocyanate (KSCN, 98%), tetrabutylammonium thiocyanate (TBAT, 98%), 4,4′-methylenediphenyldiisocyanate (MDI, 99%), 1,4-butanediol (BDO, 99%), and dibutyltin dilaurate (DBTDL, 95%) were purchased from Adamas-beta Reagent Co., Ltd. Distilled water (H_2O) was purchased from the Shanghai Yixing Trade Company. All the reagents and solvents were used as received without further purification unless otherwise stated.

General AROP Procedure. In a reaction tube (25 mL), 2 mL of DMF was added to dissolve the episulfide (2-(4-vinyl phenoxymethyl)thiirane (VPT), 2-(2-methoxy-4-vinyl phenoxymethyl)thiirane (MVPT), 2-(2-methoxy-4-allyl phenoxymethyl)thiirane (MAPT), or 2-(4-(hydroxymethyl)-phenoxymethyl)thiirane (*p*HMPT), 2.0 mmol) and TBAT (60 mg, 0.2 mmol). The solution was stirred at 40 °C for 12 h and precipitated in methanol (40 mL). It was dissolved again in 2 mL of tetrahydrofuran (THF), and the solution was dropped into methanol (40 mL). The collected product was dried under vacuum to offer the desired polythioether.

Poly(2-(4-vinyl phenoxymethyl)thiirane) (PVPT) was obtained as a white solid (353 mg, 92%). ^{1}H NMR (500 MHz, DMSO-d_6): δ (ppm) 7.25−7.24 (m, 2H, benzene), 6.76 (s, 2H, benzene), 6.64−6.58 (m, 1H, CC*H*=CH$_2$), 5.60−5.11 (m, 2H, CCH=C*H*$_2$), 4.13−4.06 (m, 2H, OC*H*$_2$CH), 3.22 (s, 1H, CH$_2$C*H*S), 3.00 (s, 2H, C*H*$_2$CHS). ^{13}C NMR (126 MHz, DMSO-d_6): δ (ppm) 158.7, 136.5, 130.6, 128.0, 115.2, 112.48, 69.8, 46.3, 34.1. M_n = 57.5 kDa, $Đ$ = 1.40.

Poly(2-(2-methoxy-4-vinyl phenoxymethyl)thiirane) (PMVPT) was obtained as a white solid (434 mg, 92%). ^{1}H NMR (500 MHz, DMSO-d_6): δ (ppm) 6.99 (s, 1H, benzene), 6.80−6.76 (d, 2H, benzene), 6.58−6.53 (m, 1H, CC*H*=CH$_2$), 5.64−5.60 (d, 1H, CCH=C*H*$_2$), 5.08−5.06 (d, 1H, CCH=C*H*$_2$), 4.09−4.04 (d, 2H, CHC*H*$_2$S), 3.73−3.66 (t, 3H, C*H*$_3$O), 3.21 (s, 1H, C*H*SCH$_2$), 3.17−3.00 (m, 2H, C*H*$_2$CHCH$_2$S). ^{13}C NMR (126 MHz, DMSO-d_6): δ (ppm) 149.6, 148.0, 136. 8, 131.1, 119.9, 119.3, 114.0, 112.9, 70.2, 55.9, 46.1, 28.6. M_n = 72.6 kDa, $Đ$ = 1.42.

Poly(2-(2-methoxy-4-allyl phenoxymethyl)thiirane) (PMAPT) was obtained as a white solid (423 mg, 90%). ^{1}H NMR (500 MHz, DMSO-d_6): δ (ppm) 6.84−6.54 (d, 3H, benzene), 5.87−5.84 (m, 1H, C*H*=CH$_2$), 5.01−4.95 (t, 2H, CH=C*H*$_2$), 4.05−3.99 (d, 2H, C*H*$_2$O), 3.60 (s, 3H, C*H*$_3$), 3.19 (s, 3H, C*H*$_2$CH=CH$_2$ and CH$_2$C*H*S), 3.05−2.92 (m, 2H, C*H*$_2$CHS). ^{13}C NMR (126 MHz, DMSO-d_6): δ (ppm) 149.8, 146.5, 138.5, 133.5, 120.4, 116.2, 114.3, 112.9, 70. 9, 56.0, 46.6, 34.0, 28.9. M_n = 48.5 kDa, $Đ$ = 1.30.

Poly(2-(4-(hydroxymethyl)phenoxymethyl)thioether) (P*p*HMPT) was obtained as a white solid (331 mg, 92%). M_n = 101.4 kDa, $Đ$ = 1.47.

Synthesis of Copolythioethers by the AROP Process. In a reaction tube (25 mL), 2.5 mL of DMF was added to dissolve the biobased thiirane (VPT, MVPT, or MAPT, 2.0 mmol), *p*HMPT (98 mg, 0.5 mmol), and TBAT (75 mg, 0.25 mmol). After being stirred at 40 °C for 12 h, the solution was precipitated in methanol (2 × 40 mL), and the collected product was dried under vacuum to obtain the copolythioether (P(VPT-*co*-*p*HMPT), P(MVPT-*co*-*p*HMPT), or P(MAPT-*co*-*p*HMPT)).

P(VPT-*co*-*p*HMPT) was obtained as a white solid (434 mg, 90%). ^{1}H NMR (500 MHz, DMSO-d_6): δ (ppm) 7.25−7.13 (m, 9H, benzene and C*H*CH$_2$), 6.77−6.56 (d, 1H, CHC*H*$_2$), 5.58−5.55 (d, 1H, CHC*H*$_2$), 5.06−5.04 (t, 2H, CHC*H*$_2$ and CH$_2$O*H*), 4.37 (s, 2H, C*H*$_2$OH), 4.11−4.05 (d, 2H, OC*H*$_2$CHS), 3.20 (s, 1H, OCH$_2$C*H*S), 2.99 (s, 2H, OCH$_2$C*H*S). ^{13}C NMR (126 MHz, DMSO-d_6): δ (ppm) 158.2, 136.4, 130.6, 128.4, 127.8, 127.2, 115.0, 114.6, 112.4, 69.7, 63.0, 46.2, 34.0. M_n = 95.8 kDa, $Đ$ = 1.50.

P(MVPT-*co*-*p*HMPT) was obtained as a white solid (499 mg, 92%). ^{1}H NMR (500 MHz, DMSO-d_6): δ (ppm) 7.11−6.56 (m, 8H, benzene and C*H*CH$_2$), 5.64−5.61 (d, 1H, CHC*H*$_2$), 5.08−5.02 (t, 2H, CHC*H*$_2$ and CH$_2$O*H*), 4.35 (s, 2H, C*H*$_2$OH), 4.12−4.08 (t, 2H, OC*H*$_2$CHS), 3.65 (s, 3H, OCH$_3$), 3.17−3.14 (t, 1H, OCH$_2$C*H*S), 3.00 (s, 2H, OCH$_2$C*H*S). ^{13}C NMR (126 MHz, DMSO-d_6): δ (ppm) 149.7, 148.1, 136.9, 131.2, 129.9, 128.4, 119.6, 114.5, 113.86, 112.7, 110.0, 70.6, 62.9, 58.0, 46.2, 33.7. M_n = 104.5 kDa, $Đ$ = 1.56.

P(MAPT-*co*-*p*HMPT) was obtained as a white solid (602 mg, 90%). ^{1}H NMR (500 MHz, DMSO-d_6): δ (ppm) 7.12−6.54 (m, 7H, benzene), 5.86−5.85 (d, 1H, CH$_2$CHC*H*$_2$), 5.01−4.95 (t, 3H, CH$_2$CHC*H*$_2$ and CH$_2$O*H*), 4.36 (s, 2H, C*H*$_2$OH), 4.06−4.00 (d, 2H, OC*H*$_2$CHS), 3.61 (s, 3H, OCH$_3$), 3.20 (s, 1H, OCH$_2$C*H*S), 2.99 (s, 2H, OCH$_2$C*H*S). ^{13}C NMR (126 MHz, DMSO-d_6): δ (ppm) 149.5, 146.4, 138.2, 133.4, 130. 8, 128.2, 120.7, 116.0, 114.4, 113.2, 70.8, 63.0, 58.0, 46.2, 33.9. M_n = 82.1 kDa, $Đ$ = 1.52.

Synthesis of Cross-Linked Copolythioethers. 1,4-Butanediol (90 mg, 1.0 mmol) and MDI (375 mg, 1.5 mmol) were put into a 25 mL three-neck flask under a N_2 atmosphere and dissolved in 2.5 mL of DMF. The polyurethane (PU) with two terminal isocyanate groups was obtained after the reaction at 60 °C for 1 h. Then, P(VPT-*co*-

https://doi.org/10.1021/acs.macromol.5c00389
Macromolecules 2025, 58, 4769−4779

Scheme 1. Synthesis of (a) Biobased Epoxide, (b) Polythioether, and (c) Cross-Linked Polythioether

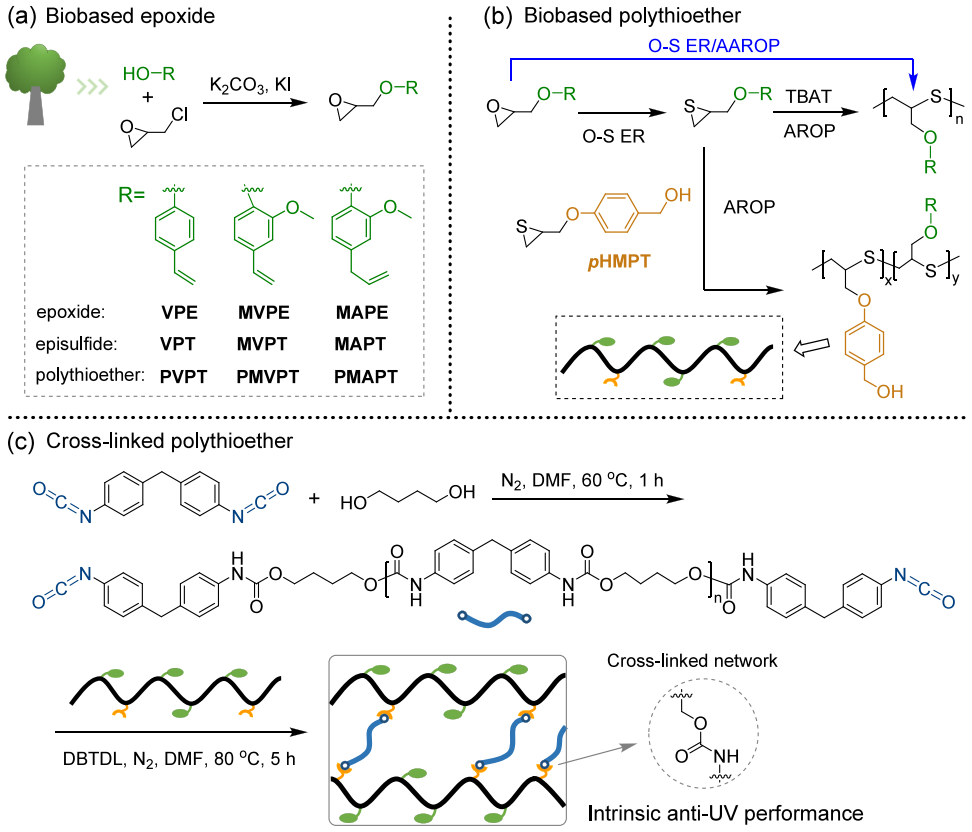

Table 1. Characteristics for Biobased Polythioethers

entry	polymer	M_n[c] (kDa)	M_w[c] (kDa)	$Đ$[c]	yield (%)	T_g[d] (°C)	T_d[e] (°C)
1[a]	PVPT	8.6	13.6	1.58	80	25	
2[a]	PMVPT	10.1	16.7	1.65	78	20	
3[a]	PMAPT	9.0	14.4	1.60	78	4	
4[b]	PVPT	57.5	80.5	1.40	92	29	
5[b]	PMVPT	72.6	103.1	1.42	92	32	275
6[b]	PMAPT	48.5	63.1	1.30	90	6	
7[b]	P*p*HMPT	101.4	149.1	1.47	92	45	
8[b]	P(VPT-*co*-*p*HMPT)	95.8	143.7	1.50	90	32	
9[b]	P(MVPT-*co*-*p*HMPT)	104.5	163.0	1.56	92	38	288
10[b]	P(MAPT-*co*-*p*HMPT)	82.1	124.8	1.52	90	15	

[a]O−S ER/AAROP procedure from epoxide: $[M]_0$ = 2 mol L^{-1}, H_2O, [M]/[TBAT] = 1:2, 40 °C, 12 h. [b]AROP procedure from episulfide: $[M]_0$ = 1 mol L^{-1}, [M]/[TBAT] (mole ratio) = 10:1, DMF, 40 °C, 12 h. [c]Determined by GPC in THF relative to monodisperse polystyrene standards and $Đ = M_w/M_n$. [d]Determined by DSC. [e]Determined by TGA.

*p*HMPT) (4.65 g, dissolved in 11 mL of DMF) and DBTDL (4 mg) were added and reacted at 80 °C for 5 h. Finally, the insoluble solid was soaked in methanol (100 mL), collected, and dried under vacuum, and the cross-linked copolythioether P(VPT-*co*-*p*HMPT)-PU was obtained.

Other cross-linked copolythioethers P(MVPT-*co*-*p*HMPT)-PU and P(MAPT-*co*-*p*HMPT)-PU were also prepared in the same procedure. The films of the copolythioether and cross-linked copolythioether were prepared by hot pressing at 80 °C under 10 MPa for 10 min.

RESULTS AND DISCUSSION

Synthesis and Characterization of Biobased Monomers. Three biobased epoxides VPE, MVPE, and MAPE were readily prepared by the etherification reaction of epichlorohydrin and biobased derivatives of 2-methoxy-4-vinylphenol, 4-vinylphenol, and UG (Scheme 1a). The experimental procedures were described in detail (see the Supporting Information), and the chemical structure of biobased epoxides was characterized by ^1H and ^{13}C NMR spectra (Figure S1). The signal peak of the phenolic hydroxyl group disappeared, and the signal peak of ethylene oxide appeared at 2.71−2.84, 3.34, and 3.81−4.34 ppm. In addition, the signal peaks of other groups all existed, which demonstrated the successful synthesis of three biobased epoxides. Their chemical structures were also confirmed by FT-IR spectroscopy (Figure S2). The peaks at 1575, 1508, and 1241 cm^{-1} belong to Ph−H and Ph−O of the benzene ring group, and the peaks at 1604 and 1022 cm^{-1} belong to C═C and C−O. Furthermore, three epoxides were further verified by mass spectra (Figures S3−S5). Novel biobased episulfides VPT, MVPT, and MAPT were then prepared though O−S ER from the above-mentioned epoxides

https://doi.org/10.1021/acs.macromol.5c00389
Macromolecules 2025, 58, 4769−4779

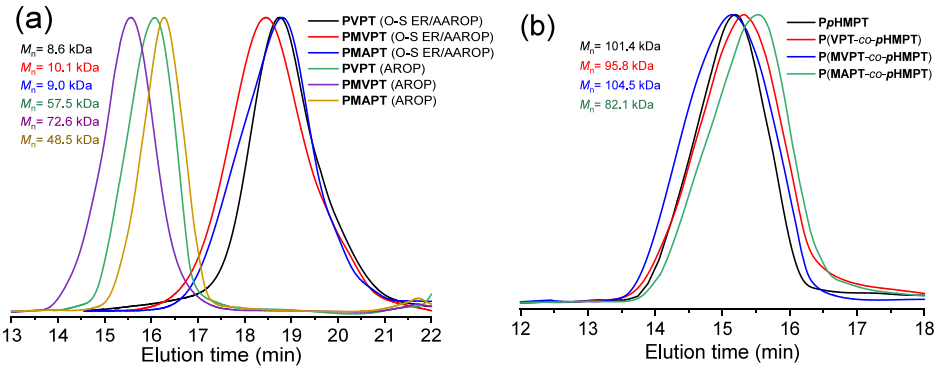

Figure 1. GPC traces of biobased polythioethers (a) and copolythioethers (b).

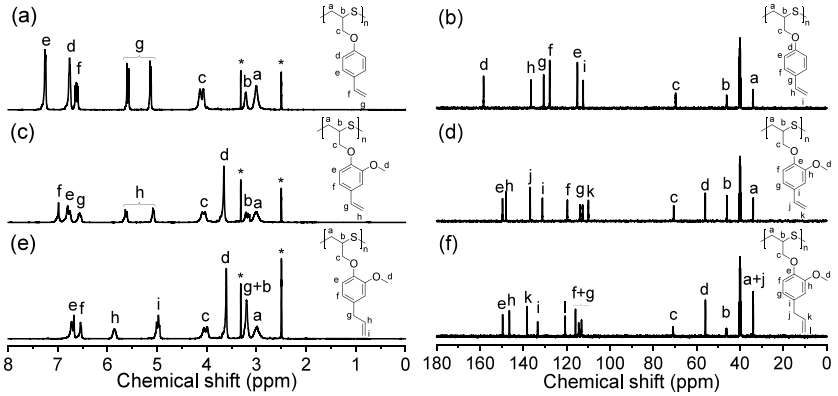

Figure 2. ^{1}H NMR (a, c, e) and ^{13}C NMR (b, d, f) spectra of PVPT (a, b), PMVPT (c, d), and PMAPT (e, f). The signals of DMSO-d_6 (2.50 ppm) and H_2O (3.30 ppm) are marked with "*" in ^{1}H NMR spectra.

and KSCN (Scheme 1b), and their chemical structure was confirmed by ^{1}H and ^{13}C NMR spectra (Figure S6). The disappearance of signal peaks belonging to ethylene oxide and the appearance of signal peaks at 4.17−3.98, 3.33, and 2.66−2.44 ppm belonging to thiirane demonstrated the completion of the O−S ER process. The signal peaks of other moieties did not change significantly, which proved the successful synthesis of three episulfides. Their chemical structure was also confirmed by FT-IR spectroscopy (Figure S7). The peaks at 818 cm^{-1} attributed to the C−S bond and the peaks at 1604, 1577, 1508, and 1241 cm^{-1} belonging to C═C, Ph−H, and Ph−O did not change significantly. Furthermore, three episulfides were further proven by the mass spectra (Figures S8−S10).

Synthesis and Characterization of Polythioethers. First, cascade O−S ER/AAROP was attempted using TBAT as both a sulfur-donating reagent and initiator at 40 °C for 12 h, and a new type of biobased polythioether was indeed produced directly from epoxide containing alkenyl groups in a one-pot procedure, which has moderate number-average molecular weight (M_n) in the range of 8.6−10.1 kDa (entries 1−3, Table 1) and relatively low dispersity ($Đ$) between 1.58 and 1.60 (Figure 1a). The reaction mechanism of the O−S ER/AAROP is shown in Scheme S1a. The poor solubility of epoxide in water led to a low or moderate M_n of polythioether obtained by the cascade O−S ER/AAROP approach, which made it difficult to expand its application. For increasing the M_n of polythioether, AROP of representative episulfide MAPT (separately prepared by the O−S ER process) was explored using DMF as a solvent and TBAT as an initiator at different conditions (entries 1−4, Table S1), and polythioether was formed with increased M_n (Figure S11). Importantly, polythioether PMAPT with high M_n, low $Đ$, and high yield was achieved under optimized conditions (entry 5, Table S1), indicating that AROP of episulfide has occurred efficiently in an open vessel, which avoided the stringent conditions required by the traditional AROP process. Based on the above results, AROP of two other biobased episulfides VPT and MVPT was carried out (entries 4−6, Table 1). As expected, the M_n of polythioethers experienced a notable increase and reached 48.5−72.6 kDa accompanied with narrowed $Đ$ of 1.30−1.42 (Figure 1a). In addition, P*p*HMPT was prepared via AROP of *p*HMPT,[38] and its M_n was further increased to 101.4 kDa (Figure 1b). In order to realize the functional application, random copolythioethers P(VPT-*co*-*p*HMPT), P(MVPT-*co*-*p*HMPT), and P(MAPT-*co*-*p*HMPT) bearing two types of functional side groups were prepared by copolymerization of *p*HMPT and the corresponding episulfide with a molar ratio of 1:4. The M_ns of copolythioethers reached 82.1−104.5 kDa, and their $Đ$ values were between 1.50 and 1.56. The molecular weight of (co)polythioethers prepared by AROP of episulfides was significantly improved compared with that by the O−S ER/AAROP procedure directly from epoxide, which makes them have the potential to achieve excellent properties.

The structure of the novel polythioethers was verified by ^{1}H and ^{13}C NMR spectra (Figure 2a−f). The disappearance of signal peaks at 3.33 and 2.66−2.44 ppm belonging to thiirane and the appearance of signal peaks at 3.22 and 3.00 ppm assigned to the main chain of polythioethers suggested the occurrence of the AROP process. The signal peaks of other moieties did not change obviously, which proved the successful

https://doi.org/10.1021/acs.macromol.5c00389
Macromolecules 2025, 58, 4769−4779

Table 2. Mechanical Properties of Biobased Polythioethers

sample	tensile strength (MPa)	elongation at break (%)	Young's modulus (MPa)	toughness (MJ m^{-3})
PVPT	7.4 ± 0.3	76 ± 2	42.10	4.21
PMVPT	5.1 ± 0.2	137 ± 3	29.28	5.64
PMAPT	3.7 ± 0.2	81 ± 2	8.67	1.89
P(VPT-*co*-*p*HMPT)	11.5 ± 0.4	651 ± 7	28.62	57.39
P(MVPT-*co*-*p*HMPT)	9.2 ± 0.4	869 ± 6	25.59	69.08
P(MAPT-*co*-*p*HMPT)	7.4 ± 0.3	1282 ± 12	10.18	83.42
P(VPT-*co*-*p*HMPT)-PU	19.1 ± 0.8	430 ± 5	40.55	55.13
P(MVPT-*co*-*p*HMPT)-PU	17.9 ± 0.4	534 ± 5	33.42	59.88
P(MAPT-*co*-*p*HMPT)-PU	14.3 ± 0.5	730 ± 6	23.79	73.95
P(MVPT-*co*-*p*HMPT)-PU first[a]	16.8 ± 0.4	503 ± 4	22.72	53.19
P(MVPT-*co*-*p*HMPT)-PU second[a]	15.2 ± 0.5	475 ± 4	19.63	46.04
P(MVPT-*co*-*p*HMPT)-PU third[a]	12.4 ± 0.5	423 ± 6	17.44	35.62
P(MVPT-*co*-*p*HMPT)-MDI	19.3 ± 0.4	170 ± 4	42.27	20.04

[a]Reprocessing: 80 °C, 10 MPa, 10 min.

synthesis of three polythioethers. Subsequently, the structure of copolythioethers was analyzed by ^{1}H and ^{13}C NMR spectra (Figures S12−S14). The signal peaks belonging to the hydroxyl group and the methylene group of P*p*HMPT appeared separately at 5.06−5.04 and 4.37 ppm, and the signal peaks assigned to three biobased polythioethers had no significant change, indicating the formation of copolythioethers. By integral calculation, the molar ratio of two different units in copolythioethers was determined to be 1:3.85−4.00, which was close to the feed ratio (1:4) of two monomers. Notably, the observed signal integration ratio of protons on the hydroxyl group and adjacent methylene group was consistent with the proton molar ratio of 1:2, meaning that the sulfanion (S^-) has good tolerance to weak acidic protons of functional groups, and thus, no chain transfer reaction occurred between the S^- at the living chain end and the hydroxyl group under weakly alkaline conditions (pH ≈ 8).

MALDI-TOF mass spectroscopy was employed to further validate the structure of polythioether, and low-molecular-weight PMAPT (M_n = 8.1 kDa) was selected for measurement. The equidistant peaks, such as 7613.951, 7850.041, 8086.131, and 8322.221 *m*/*z*, showed a molecular mass interval of 236.090 *m*/*z* (Figure S15), which was in good agreement with the molecular mass of the MAPT unit (236.087 *m*/*z*). The value of all high-intensity signals corresponded to [SCN+($C_{13}H_{16}O_2S$)$_n$+H], demonstrating the $^-$SCN moiety as a nucleophile to initiate AROP. It was previously proven that the complexation between the cation of TBAT ($Bu_4N^+{}^-SCN$) and the sulfur atom of thiirane played a key role in activating the thiirane ring and strengthening the nucleophilicity of $^-$SCN, which could effectively initiate AROP of episulfide and promote the overall chain growth to obtain polythioether.[38] TBAT might exist mainly as ion pairs in DMF, which did not have enough ability to trigger the AROP of episulfide. When the cation Bu_4N^+ was complexed with a sulfur atom, it could not only activate the thiirane but also facilitate the dissociation of thiocyanate into free ions and enhance the nucleophilicity of anion $^-$SCN to initiate AROP (Scheme S1b). It is worth noting that the reaction mechanism was slightly different from the chain growth process observed in classical AROP because the dissociation degree of thiocyanate significantly influenced the AROP behavior, and its degree of polymerization was primarily determined by the molar ratio of the monomer to the dissociated $^-$SCN concentration rather than the initial TBAT concentration. Therefore, the initial polymerization rate was expected to be lower than that of conventional AROP, and the M_n of polythioether showed a gradual increase as the reaction time accompanied with the widening of $Đ$ (Table S1).

Synthesis and Characterization of Cross-Linked Copolythioethers. PU has the advantages of high elasticity and exceptional biocompatibility and can be widely used in biomedicine, automotive components, sports equipment, and other fields due to the diversity of formulations.[39−41] As a cross-linking agent, the PU prepolymer has the potential to significantly improve the mechanical properties and thermal stability of polymer materials. Therefore, excess MDI and butanediol were allowed to react at 60 °C for 1 h to yield the PU prepolymer with reactive chain ends of isocyanates and an M_n of 2.5 kDa (Figure S16). Then, the cross-linked copolythioether was synthesized at 80 °C for 5 h using DBTDL as the catalyst and the PU prepolymer as the cross-linking agent (Scheme 1c). The structure of cross-linked copolythioether P(MVPT-*co*-*p*HMPT)-PU was characterized by FT-IR spectroscopy (Figure S17a). The presence of two characteristic peaks at 3315 and 1530 cm^{-1} belonged to the stretching and bending vibration peaks of −NH (Figure S17b), respectively, which indicated the successful formation of the carbamate group (−NHCOO−). Moreover, the absorption peak at 2240−2280 cm^{-1} belonging to −NCO was not observed, suggesting that it was reacted with −OH of copolythioethers successfully. The cross-linking density of cross-linked copolythioethers was calculated to be 2.4−2.7 × 10^{-4} mol cm^{-3}, and the sol fraction was less than 19% (Figure S18).

Thermal Properties of Polythioethers. The thermal properties of polythioethers were inspected by differential scanning calorimetry (DSC) and thermogravimetric analysis (TGA) techniques. PVPT with rigid side groups of styrene had a glass transition temperature (T_g) of 25 °C (Figure S19). The T_g of PMVPT was reduced to 20 °C due to the presence of methoxyl in the side groups. The introduction of the allyl and methoxyl into the side groups of PMAPT resulted in the lower T_g of 4 °C. The M_n of polythioethers prepared by AROP of episulfides significantly increased, leading to the increase in T_g (Figure S20). Among them, the M_n of PMVPT increased from 10.1 to 72.6 kDa, accompanied with the increase in T_g from 20 to 32 °C. The T_g of P*p*HMPT prepared by a cascade O−S ER/AAROP approach was 35 °C,[38] while it was raised to 45 °C because of the obviously increased molecular weight. Copolythioethers have the T_g in the range of 15−38 °C.

https://doi.org/10.1021/acs.macromol.5c00389
Macromolecules 2025, 58, 4769−4779

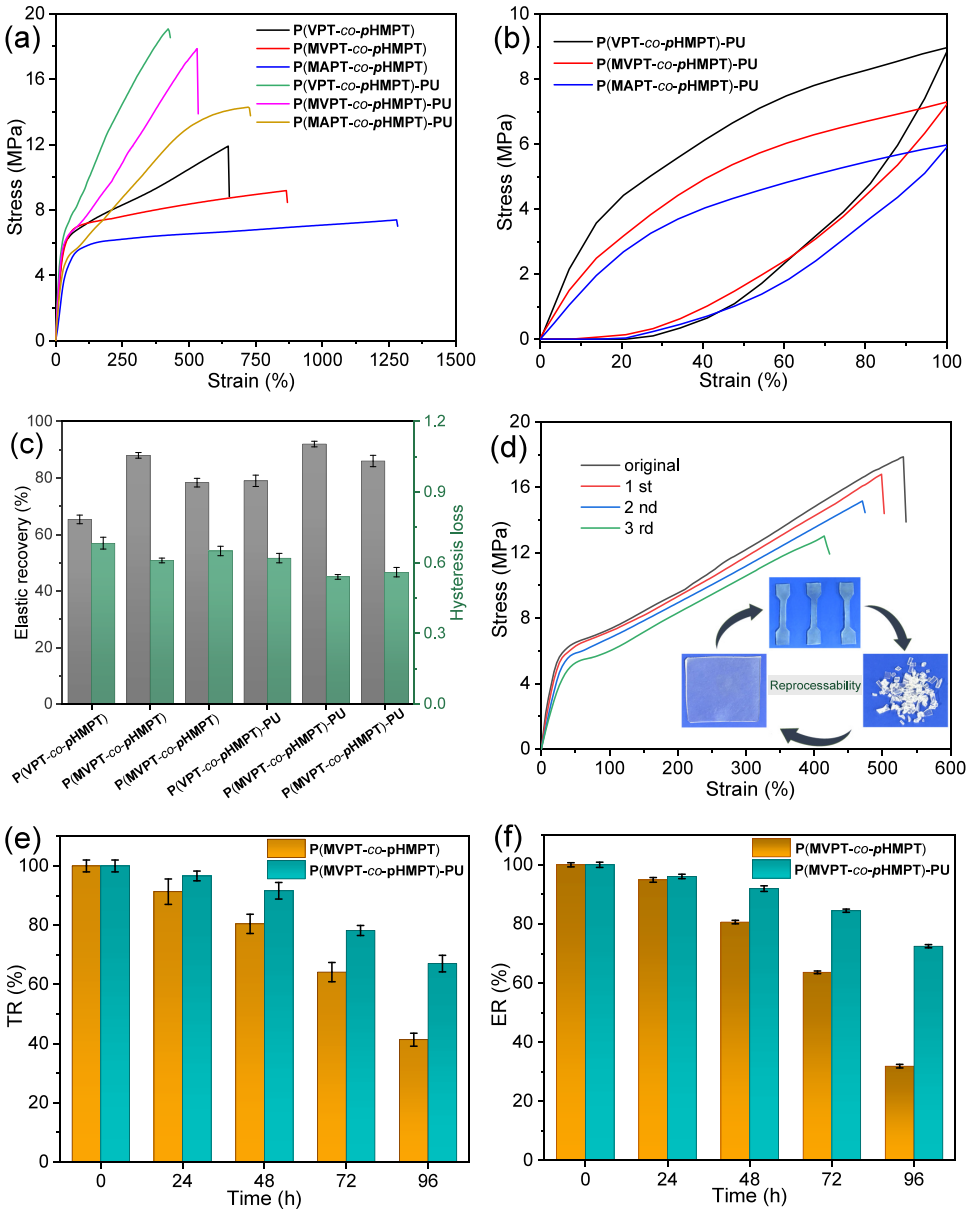

Figure 3. Stress−strain curves of copolythioethers and cross-linked copolythioethers (a). Tensile loading−unloading cycles of cross-linked copolythioethers (b). Bar graph summarizing elastic recovery and hysteresis loss of copolythioethers (c). Stress−strain curves of P(MVPT-*co*-*p*HMPT)-PU after several reprocessing (d). Tensile strength retention (TR) (e) and elongation at break retention (ER) (f) of P(MVPT-*co*-*p*HMPT) and P(MVPT-*co*-*p*HMPT)-PU at each interval of 24 h under UV irradiation.

TGA was used to evaluate the thermal stability of different polythioethers with the core structure of 2-methoxy-4-vinylphenol, and the decomposition temperature (T_d) at 5% weight loss was obtained (Figure S21). PMVPT has a T_d of 275 °C, and the T_d of P(MVPT-*co*-*p*HMPT) increased to 288 °C due to the increase in the molecular weight of the copolymer and the existence of hydrogen bond interaction between the side groups. The T_d of P(MVPT-*co*-*p*HMPT)-PU further increased to 296 °C, indicating that the thermal stability of polythioether was improved by a cross-linking reaction.

Mechanical Properties of Polythioethers. The mechanical properties of polythioethers were described using stress−strain curves, Young's modulus was obtained by the ratio of stress to strain at the initial elastic deformation stage, and the toughness was calculated by the integral area of the stress−strain curve. Although polythioethers PVPT, PMVPT, and PMAPT obtained by AROP have higher molecular weight, their tensile strength ranged within 3.7−7.4 MPa (Table 2), and the elongation at break ranged from 76 to 137% (Figure S22a); such mechanical properties were not good enough to meet the requirements of daily application. The introduction of *p*HMPT units with hydroxyl groups into copolythioethers improved their mechanical properties significantly because the increased molecular weight of copolythioethers and the hydrogen bond interaction enhanced the intermolecular force (Scheme S2a). For P(VPT-*co*-*p*HMPT), the tensile strength of 11.5 MPa, the elongation at break of 651%, and the toughness of 57.39 MJ m^{-3} were much higher than those of PVPT (Figure 3a). The tensile strength of P(MVPT-*co*-*p*HMPT) was 9.2 MPa, the elongation at break was 869%, and the toughness was 69.08 MJ m^{-3}. The tensile strength of P(MAPT-*co*-

https://doi.org/10.1021/acs.macromol.5c00389
Macromolecules 2025, 58, 4769−4779

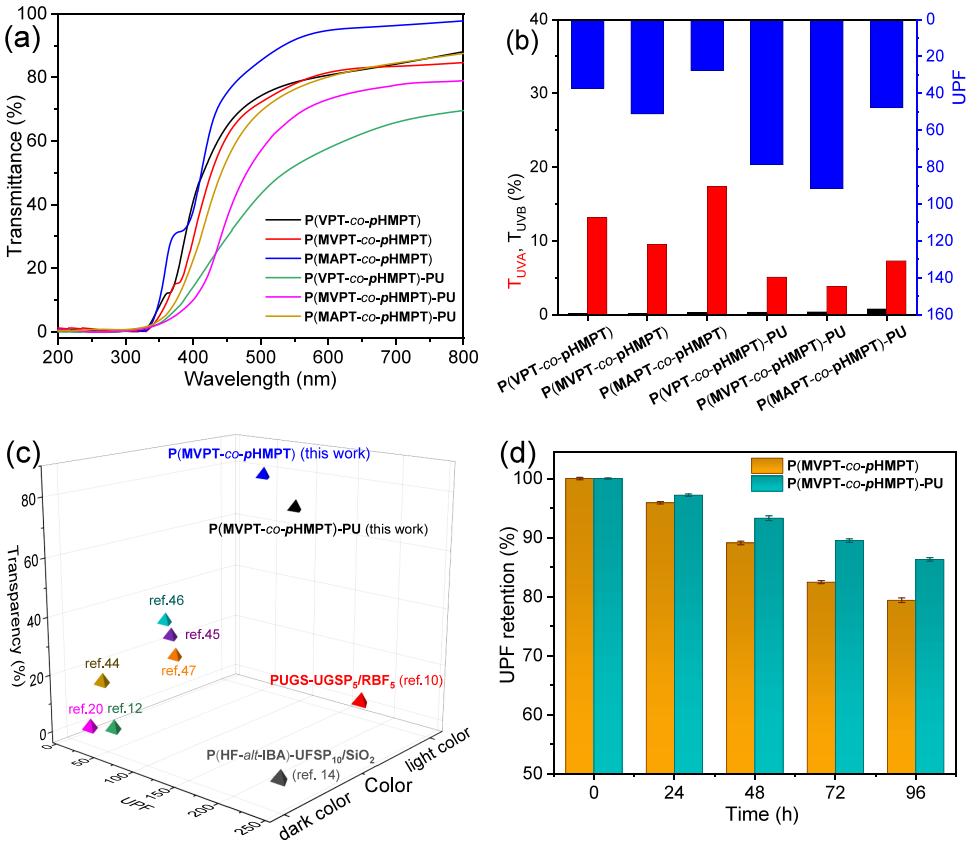

Figure 4. UV-light transmittance curves of copolythioethers and cross-linked copolythioether films (a). UPF, T_{UVB}, and T_{UVA} values of poly(thioether) films (b). Comparison for color, transparency, and UPF values of different biobased anti-UV materials (c). UPF retentions of P(MVPT-*co*-*p*HMPT) and P(MVPT-*co*-*p*HMPT)-PU at each interval of 24 h under UV irradiation (d).

*p*HMPT) was 7.4 MPa, the elongation at break increased to 1282%, and the toughness reached 83.42 MJ m^{-3}. After cross-linking with the PU prepolymer, the tensile strength of cross-linked copolythioethers was significantly improved (14.3−19.1 MPa), and the elongation at break varied from 430 to 730%, but the toughness decreased correspondingly (Figure S23). The resilience of modified polythioether was tested by tensile loading−unloading cycling tests, the hysteresis loss was obtained by the area of tensile loading−unloading cycle curves, and the results are listed in Table S2. The elastic recovery rate of copolythioether was between 65 and 88%, and the hysteresis loss ranged from 0.61 to 0.68 (Figure S22b). Moreover, the elastic recovery rate of cross-linked copolythioether improved obviously (79−92%), and the hysteresis loss was slightly reduced (0.54−0.62), which gave it better durability and extended service life (Figure 3b,c). Among them, P(MVPT-*co*-*p*HMPT)-PU exhibited excellent resilience, with the highest elastic recovery rate of 92% and the lowest hysteresis loss of 0.54. Taking P(MVPT-*co*-*p*HMPT) as an example, the cross-linked copolythioether P(MVPT-*co*-*p*HMPT)-MDI was also prepared using MDI (10 wt %, the same amount with the PU prepolymer) as the cross-linking agent. Its tensile strength increased to 19.3 MPa, while the elongation at break was lowered to 170% (Figure S24). Compared with the PU prepolymer, the cross-linked structure formed by MDI was relatively tight, so the toughness of P(MVPT-*co*-*p*HMPT)-MDI decreased significantly, and the resilience was lost. The hydrogen bond interaction and hydroxyl-mediated transcarbamoylation would make the polymer possible to reprocess.[42,43] The cross-linked P(MVPT-*co*-*p*HMPT)-PU strips were cut into pieces and then reshaped at 80 °C under 10 MPa for 10 min to obtain a smooth sheet (Figure 3d). After three hot pressing cycles, the cross-linked polymer network still remained intact, and the tensile strength and elongation at break of P(MVPT-*co*-*p*HMPT)-PU could be maintained at 12.4 MPa and 423%, respectively. These observations indicated that the existence of dynamically reversible hydrogen bond interaction and hydroxyl-mediated transcarbamoylation allowed the cross-linked copolythioether to be reprocessable (Scheme S2b,c).

Dynamic Mechanical Properties of Modified Polythioethers. The dynamic mechanical properties of copolythioether and cross-linked copolythioether were investigated by dynamic mechanical analysis (DMA), and the dependence of the storage modulus (E') and loss factor (tan δ) on temperature was presented. The increased interaction between molecular chains endowed materials with better store energy when they get stressed; consequently, the cross-linked copolythioethers have higher E' than copolythioethers (Figure S25a). According to Figure S25b, the damping peak of tan δ for the three copolythioethers ranged within 0.62−0.78, which was higher than that (0.48−0.59) of the corresponding cross-linked copolythioethers (Table S3). The reason was that the cross-linking reduced the degree of motion freedom of the molecular segments, thereby reducing energy loss. The cross-linked structure working with the hydrogen bond interaction could increase the internal friction of cross-linked copolythioether chains during movement and therefore widened their maximum damping temperature.

https://doi.org/10.1021/acs.macromol.5c00389
Macromolecules 2025, 58, 4769−4779

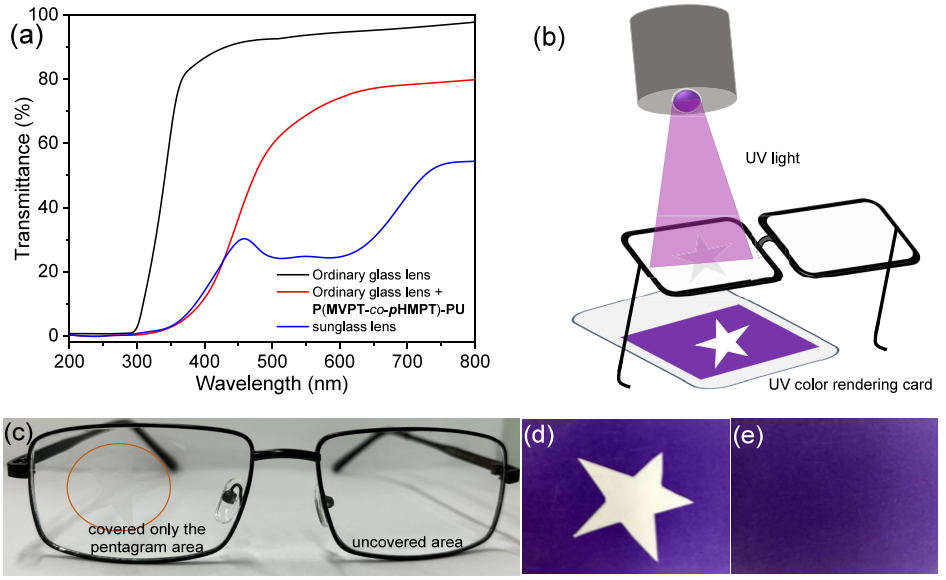

Figure 5. UV-light transmittance curves of the ordinary glass lens, ordinary glass lens covered with a P(MVPT-*co*-*p*HMPT)-PU film, and commercial sunglass lens (a). Schematic diagram of anti-UV glasses irradiated with a UV lamp (365 nm, 200 W) (b). Digital picture of the glass lens covered with a P(MVPT-*co*-*p*HMPT)-PU film (c). Digital picture of the UV color rendering card was put under the glass lens after UV-light exposure. The glasses were partially covered with an anti-UV film (d) and uncovered with an anti-UV film (e).

Anti-UV Performance of Polythioethers. The absorption peaks in the UV−vis spectra of four epoxides ranged from 261 to 297 nm (Figure S26a), and the UV absorption peaks of the corresponding episulfides were redshifted to 268−309 nm. The primary reason was that the utilization of sulfur atoms as electron donors may subsequently affect the electron density of episulfide and afford nonconjugated lone-pair electrons, which are capable of generating a new absorption center. The UV absorption peaks of polythioethers were further redshifted to 278−314 nm (Figure S26b). The anti-UV performance of the prepared polythioether films with a thickness of 50 μm was described by the UV transmittance curves. The average transmittance values of UVA light (T_{UVA}) and UVB light (T_{UVB}) and the UV protection factor (UPF) were calculated, and the lower the transmittance, the higher the UPF value. According to the conventional standard, the UPF value of the anti-UV material must be greater than 40, and the T_{UVA} must be less than 5%. PVPT containing a styrene pendant can block nearly 99% of UVB light (T_{UVB} = 1.01%) and 97% of UVA light (T_{UVA} = 3.05%), and the calculated UPF value was as high as 68, which showed an effective UV resistance (Figure S26c and Table S4), while its transparency (transmittance at 550 nm) was only 22%. The strong and regular face-to-face $\pi-\pi$ stacking between the conjugated styryl pendants in PVPT may induce local ordered aggregation of macromolecular chains and form high-density regions. These ordered regions increased light scattering and enhanced the refractive index difference, thereby reducing the transparency of the film. Because of the wider UV absorption range, the T_{UVA} and T_{UVB} of the PMVPT film were reduced to 2.40 and 0.64%, respectively. The calculated UPF value was up to 98.2, and its transparency was increased to 45%. Delightingly, PMAPT exhibited a high UPF value of 49.4 and demonstrated a good transparency at 86%. For balancing the transparency and anti-UV performance, the hydroxyl-functionalized polythioether P*p*HMPT was considered to tune the properties, and it showed an excellent transparency of 94% and good protection in UVB light due to its limited UV absorption range but poor protection in UVA light and a low UPF value of 14.5. Therefore, the T_{UVA} values of the *p*HMPT unit-containing copolythioethers were enlarged (9.55−17.4%), and the UPF values were between 51.2 and 27.7 (Figure 4a,b). For copolythioethers, the transparency has significantly improved and reached to 78−92%. After cross-linking by PU, the T_{UVA} and T_{UVB} values of the cross-linked copolythioethers were obviously reduced, mainly owing to the introduction of the cross-linked structure and the enhanced intermolecular interaction, which increased their UV absorption capacity (Figure S26d). Among them, P(MVPT-*co*-*p*HMPT)-PU showed the T_{UVA} of 3.84% and the T_{UVB} of 0.40%, and thus, the calculated UPF value reached to 91.8, which could be considered as an excellent anti-UV material. More importantly, unlike other colored or opaque anti-UV films (Figure 4c),[10,12,14,20,44−47] the P(MVPT-*co*-*p*HMPT)-PU film was colorless and transparent with a light transmittance of more than 68% in the visible range and could be used as an anti-UV material in various fields where colorless and transparent are required in human production and life.

Anti-UV Aging Performance of Modified Copolythioethers. P(MVPT-*co*-*p*HMPT)-PU has excellent anti-UV performance and good mechanical properties; therefore, this film was expected to have good anti-UV aging performance. The P(MVPT-*co*-*p*HMPT) and P(MVPT-*co*-*p*HMPT)-PU films were tested to evaluate and compare the effects of cross-linking modification on the anti-UV aging performance of polythioethers. The samples were exposed to high-intensity UV light for 96 h; simultaneously, their UV transmittance curves and mechanical properties were tested at each interval of 24 h. The T_{UVA} and T_{UVB} of copolythioether films increased, the UPF value decreased, and thus, the UPF retention decreased. This was mainly because UV irradiation had the capacity to break the covalent bonds in polymer chains, initiating a photooxidation process that consequently impaired the anti-UV performance of polythioether.[8] After long-term UV exposure for 96 h, the UPF of P(MVPT-*co*-*p*HMPT) reduced to 40.7, its UPF retention was 79.4% (Figure S27a),

https://doi.org/10.1021/acs.macromol.5c00389
Macromolecules 2025, 58, 4769−4779

and the transparency of the film increased from 78 to 84% (Table S5). As expected, P(MVPT-*co*-*p*HMPT)-PU still had good anti-UV performance after 96 h, its UPF was 79.2, UPF retention was 86.3%, and transparency was 70% (Figure S27b). It could be clearly observed from Figure 4d that the UPF retention of the cross-linked copolythioether films was significantly higher than that of the uncross-linked copolythioether films (Table S5) due to the relatively stable covalent cross-linked network. The anti-UV aging performance of two kinds of copolyethioethers was further compared by the changed mechanical properties. The tensile strength and elongation at break of copolythioether strips showed a continuous decline with the extension of irradiation time. As shown in Figure 3e,f and Table S6, after UV irradiation for 96 h, the mechanical properties of P(MVPT-*co*-*p*HMPT) significantly declined (Figure S28a), with a tensile strength retention (TR) of 41% (from 9.2 to 3.8 MPa) and an elongation at break retention (ER) of 32% (from 869 to 277%); P(MVPT-*co*-*p*HMPT)-PU still maintained good mechanical properties, and its tensile strength and elongation at break were reduced to 12 MPa (TR = 67%) and 387% (ER = 72%) (Figure S28b). These results showed that the cross-linked copolythioether could better resist the damage of UV light to slow down the speed of photodegradation and prolong its service life. The structural change of P(MVPT-*co*-*p*HMPT)-PU before and after UV irradiation for 96 h was verified by FT-IR spectroscopy (Figure S29a). The peaks at 3370, 3315, 1604, and 1530 cm^{-1} weakened, indicating that the photooxidation process of OH, NH, and C=C bonds occurred. It was observed that the peaks at 2930−2857 and 1034 cm^{-1} showed a decreasing trend, while the peaks at 1683 and 1648 cm^{-1} increased (Figure S29b), predicating the formation of a new carbonyl-containing structure in polythioether by UV irradiation in the presence of oxygen. The peaks at 818 cm^{-1} decreased slightly, and a new peak at 1170 cm^{-1} (assigned to S=O) was observed, suggesting that a small fraction of C−S bonds underwent photooxidation.

Application of Anti-UV Copolythioether in UV Protection. It is crucial to protect the human body from excessive UV-light exposure, as overexposure can lead to significant health issues such as cancer and cataracts. Figure 5a shows the UV-light transmittance curves of an ordinary glass lens, an ordinary glass lens covered with a P(MVPT-*co*-*p*HMPT)-PU film, and a commercial sunglass lens. Ordinary glass lens has very good light transmission in the visible-light range, but the UV absorption capacity is insufficient, and therefore, it does not have UV protection. In addition, high transparency can cause glare when light hits the lens, which resulted in the reduced visual clarity and increased eye fatigue. Sunglass lens has anti-UV performance, but the view may be slightly dimmed because of low transparency. The lens covered with the P(MVPT-*co*-*p*HMPT)-PU film has good transparency in the range of visible light and good anti-UV performance. To express the anti-UV performance of the lens covered with the P(MVPT-*co*-*p*HMPT)-PU film more intuitively, the film was cut into a pentagram shape and covered on the surface of the glass lens (Figure 5b,c). Then, the lens covered with a pentagram-shaped P(MVPT-*co*-*p*HMPT)-PU film was placed above the UV color rendering card, and a UV lamp was turned on to irradiate the lens and the card. It could be clearly observed that the sensing area of the UV color rendering card that was not protected by the pentagonal anti-UV film had strong UV radiation, while the UV color rendering card that was protected by the pentagonal anti-UV film had little change (Figure 5d). In addition, the UV color rendering card was placed under the lens without covering the anti-UV film, and its entire sensing area turned purple after exposure to identical UV irradiation conditions (Figure 5e). Moreover, the refractive index (n_d, n value at the wavelength of 587.6 nm) of the P(MVPT-*co*-*p*HMPT)-PU film was measured to be 1.633 by a spectroscopic ellipsometer (Figure S30). In comparison, commercially available plastics such as polystyrene (PS) and aromatic polycarbonate (PC) have n_ds of 1.59 and 1.58, respectively.[48] The Abbe number (V_d) of the anti-UV film was calculated to be 31, which meets the range of V_d values (30−60) required for making visual optical materials. Therefore, the colorless and transparent anti-UV film prepared in this work can be used in the manufacture of lenses, which can prevent UV-light damage to the eyes and prevent cataracts effectively.

CONCLUSIONS

Three epoxides were synthesized from biobased aromatic derivatives and used to prepare the corresponding episulfides by O−S ER with thiocyanate. A new class of high-molecular-weight biobased polythioethers were obtained by AROP of episulfides, using TBAT as the initiator in an open vessel and an undried polar solvent. They possessed high a M_n of 48.5−104.5 kDa and displayed wide T_g ranging from 6 to 45 °C. In addition, the cross-linked copolythioethers with enhanced mechanical properties and good reprocessability and the anti-UV performance were improved by the cross-linking reaction of the poly(hydroxyl thioether) segment with a long-chain isocyanate. They exhibited an excellent tensile strength of 14.3−19.1 MPa, the elongation at break ranged from 430 to 730%, and the UPF value was between 47.9 and 91.8. The representative cross-linked copolythioether P(MVPT-*co*-*p*HMPT)-PU film was colorless and transparent with outstanding intrinsic anti-UV performance. Furthermore, the cross-linked copolythioether has better resilience, reduced hysteresis loss, and relatively stable resistance to UV aging, which made it possible for it to have better durability and service life. This work not only provided a simple and effective strategy for obtaining functional polythioether with high molecular weight from renewable resources but also presented a sustainable alternative for manufacturing optical materials.

ASSOCIATED CONTENT

Supporting Information

The Supporting Information is available free of charge at https://pubs.acs.org/doi/10.1021/acs.macromol.5c00389.

Experimental procedures; calculation equations; tables; schemes; NMR, IR, MS, and UV−vis absorption and transmittance spectra; MALDI-TOF mass spectrum; refractive index curve; GPC traces; stress−strain curves; DSC, TGA, and DMA curves (PDF)

AUTHOR INFORMATION

Corresponding Authors

Xiaojuan Liao − *School of Chemistry and Molecular Engineering, East China Normal University, Shanghai 200241, China;* orcid.org/0000-0002-6046-8831; Email: xjliao@chem.ecnu.edu.cn

Meiran Xie − *School of Chemistry and Molecular Engineering, East China Normal University, Shanghai 200241, China;*

https://doi.org/10.1021/acs.macromol.5c00389
Macromolecules 2025, 58, 4769−4779

orcid.org/0000-0002-7411-3927; Email: mrxie@chem.ecnu.edu.cn

Authors

Qiubo Wang − *School of Chemistry and Molecular Engineering, East China Normal University, Shanghai 200241, China*

Xinyu Hu − *School of Chemistry and Molecular Engineering, East China Normal University, Shanghai 200241, China*

Min Yan − *School of Chemistry and Molecular Engineering, East China Normal University, Shanghai 200241, China*

Xingyu Luo − *School of Chemistry and Molecular Engineering, East China Normal University, Shanghai 200241, China*

Complete contact information is available at: https://pubs.acs.org/10.1021/acs.macromol.5c00389

Notes

The authors declare no competing financial interest.

■ ACKNOWLEDGMENTS

The authors thank the National Natural Science Foundation of China (grant numbers 21871091 and 21774033) for financial support of this research project.

■ REFERENCES

(1) Zhang, H.; Cheng, X.; Liu, C. P.; Liu, Z. J.; Liu, L.; Feng, C.; Ju, J.; Yao, X. Ultraviolet-blocking polymers and composites: recent advances and future perspectives. *J. Mater. Chem. A* **2024**, *12*, 32638−32664.

(2) Wang, D. N.; Gu, Y. J.; Feng, S.; Yang, W. S.; Dai, H. Q.; Xiao, H. N.; Han, J. Q. Lignin-containing biodegradable UV-blocking films: A review. *Green Chem.* **2023**, *25*, 9020−9044.

(3) Mondal, S. Nanomaterials for UV protective textiles. *J. Ind. Text.* **2022**, *51*, 5592S.

(4) Sander, M.; Sander, M.; Burbidge, T.; Beecker, J. The efficacy and safety of sunscreen use for the prevention of skin cancer. *Can. Med. Assoc. J.* **2020**, *192*, E1802−E1808.

(5) Rather, L. J.; Shabbir, M.; Li, Q.; Mohammad, F. Coloration, UV protective, and antioxidant finishing of wool fabric via natural dye extracts: Cleaner production of bioactive textiles. *Environ. Prog. Sustainable Energy* **2019**, *38*, 13187.

(6) Gore, A. H.; Prajapat, A. L. Biopolymer nanocomposites for sustainable UV protective packaging. *Front. Mater.* **2022**, *9*, No. 855727.

(7) Sani, M. A.; Khezerlou, A.; Tavassoli, M.; Abedini, A. H.; McClements, D. J. Development of sustainable UV-screening food packaging materials: A review of recent advances. *Trends Food Sci. Technol.* **2024**, *145*, No. 104366.

(8) Huang, G. S.; Yao, C. X.; Huang, M. M.; Zhou, J. J.; Hao, X. G.; Ma, X. J.; He, S. Q.; Liu, H.; Liu, W. T.; Zhu, C. S. Colorless, transparent, and high-performance polyurethane with intrinsic ultraviolet resistance and its anti-UV mechanism. *ACS Appl. Mater. Interfaces* **2023**, *15*, 18300−18310.

(9) Fan, L. X.; Chen, L.; Zhang, H. Y.; Xu, W. H.; Wang, X. L.; Xu, S.; Wang, Y. Z. Dual photo-responsive diphenylacetylene enables PET in-situ upcycling with reverse enhanced UV-resistance and strength. *Angew. Chem., Int. Ed.* **2023**, *62*, No. e202314448.

(10) Wang, Q. B.; Hu, X. Y.; Wang, S. Y.; Sun, R. Y.; Liao, X. J.; Xie, M. R. Eugenol-based polyester and its bamboo fiber composite with enhanced mechanical and anti-ultraviolet properties. *Polym. Chem.* **2024**, *15*, 4852−4863.

(11) Suh, H. W.; Lewis, J.; Fong, L.; Ramseier, J. Y.; Carlson, K.; Peng, Z. H.; Yin, E. S.; Saltzman, W. M.; Girardi, M. Biodegradable bioadhesive nanoparticle incorporation of broad-spectrum organic sunscreen agents. *Bioeng. Transl. Med.* **2019**, *4*, 129−140.

(12) Xie, W. J.; Pakdel, E.; Liu, D.; Sun, L.; Wang, X. G. Waste-hair-derived natural melanin/TiO_2 hybrids as highly efficient and stable UV-shielding fillers for polyurethane films. *ACS Sustainable Chem. Eng.* **2020**, *8*, 1343−1352.

(13) Liu, H. Q.; Hu, D. C.; Chen, X. J.; Ma, W. S. Surface engineering of nanoparticles for highly efficient UV-shielding composites. *Polym. Adv. Technol.* **2021**, *32*, 6−16.

(14) Wang, Q. B.; Hu, X. Y.; Wang, S. Y.; Liao, X. J.; Sun, R. Y.; Liu, Q. C.; Xie, M. R. Anti-ultraviolet biobased polyesters synthesized by acyclic diene metathesis polymerization. *Macromolecules* **2024**, *57*, 5849−5859.

(15) Krause, M.; Frederiksen, H.; Sundberg, K.; Jorgensen, F. S.; Jensen, L. N.; Norgaard, P.; Jorgensen, C.; Ertberg, P.; Juul, A.; Drzewiecki, K. T.; Skakkebaek, N. E.; Andersson, A. M. Presence of benzophenones commonly used as UV filters and absorbers in paired maternal and fetal samples. *Environ. Int.* **2018**, *110*, 51−60.

(16) Santos, B. A. M. C.; da Silva, A. C. P.; Bello, M. L.; Gonçalves, A. S.; Gouvêa, T. A.; Rodrigues, R. F.; Cabral, L. M.; Rodrigues, C. R. Molecular modeling for the investigation of UV absorbers for sunscreens: Triazine and benzotriazole derivatives. *J. Photoch. Photobio. A* **2018**, *356*, 219−229.

(17) Panchal, S. S.; Vasava, D. V. Biodegradable polymeric materials: Synthetic approach. *ACS Omega* **2020**, *5*, 4370−4379.

(18) Zhong, B. C.; Tang, Y. H.; Chen, Y. J.; Luo, Y. F.; Jia, Z. X.; Jia, D. M. Improvement of UV aging resistance of PBAT composites with silica-immobilized UV absorber prepared by a facile method. *Polym. Degrad. Stab.* **2023**, *211*, No. 110337.

(19) Gaspar, R.; Fardim, P. Lignin-based materials for emerging advanced applications. *Curr. Opin. Green Sust.* **2023**, *41*, No. 100834.

(20) Zheng, T. R.; Yang, L.; Zhang, X. F.; Yao, J. F. Conversion of corncob residue to sustainable lignin/cellulose film with efficient ultraviolet-blocking property. *Ind. Crop. Prod.* **2023**, *196*, No. 116517.

(21) Li, S. X.; Li, M. F.; Bian, J.; Wu, X. F.; Peng, F.; Ma, M. G. Preparation of organic acid lignin submicrometer particle as a natural broad-spectrum photo-protection agent. *Int. J. Biol. Macromol.* **2019**, *132*, 836−843.

(22) Ratanasumarn, N.; Chitprasert, P. Cosmetic potential of lignin extracts from alkaline-treated sugarcane bagasse: Optimization of extraction conditions using response surface methodology. *Int. J. Biol. Macromol.* **2020**, *153*, 138−145.

(23) Kerosenewala, J.; Vaidya, P.; Ozarkar, V.; Shirapure, Y.; More, A. P. Eugenol: Extraction, properties and its applications on incorporation with polymers and resins-a review. *Polym. Bull.* **2023**, *80*, 7047−7099.

(24) Zhang, X.; Cai, Y.; Zhang, X.; Aziz, T.; Fan, H.; Bittencourt, C. Synthesis and characterization of eugenol-based silicone modified waterborne polyurethane with excellent properties. *J. Appl. Polym. Sci.* **2021**, *138*, 50515.

(25) Watanabe, H.; Takahashi, M.; Kihara, H.; Yoshida, M. Biobased coatings based on eugenol derivatives. *ACS Appl. Bio Mater.* **2018**, *1*, 808−813.

(26) Le Luyer, S.; Quienne, B.; Bouzaid, M.; Guégan, P.; Caillol, S.; Illy, N. Bio-based poly(ester-*alt*-thioether)s synthesized by organo-catalyzed ring-opening copolymerizations of eugenol-based epoxides and *N*-acetyl homocysteine thiolactone. *Green Chem.* **2021**, *23*, 7743−7750.

(27) Molina-Gutiérrez, S.; Manseri, A.; Ladmiral, V.; Bongiovanni, R.; Caillol, S.; Lacroix-Desmazes, P. Eugenol: A promising building block for synthesis of radically polymerizable monomers. *Macromol. Chem. Phys.* **2019**, *220*, No. 1900179.

(28) Llevot, A.; Grau, E.; Carlotti, S.; Grelier, S.; Cramail, H. ADMET polymerization of bio-based biphenyl compounds. *Polym. Chem.* **2015**, *6*, 7693−7700.

(29) Li, Y.; Hu, B.; Fu, H.; Zhang, Z. X.; Guo, Z. T.; Zhou, G. Z.; Zhu, L. J.; Liu, J.; Lu, Q. Fast pyrolysis of bagasse catalyzed by mixed alkaline-earth metal oxides for the selective production of 4-vinylphenol. *J. Anal. Appl. Pyrol.* **2022**, *164*, No. 105531.

(30) Mishra, S.; Sachan, A.; Vidyarthi, A. S.; Sachan, S. G. Transformation of ferulic acid to 4-vinyl guaiacol as a major

metabolite: a microbial approach. *Rev. Environ. Sci. Biotechnol.* **2014**, *13*, 377−385.
(31) Huang, M. Q.; Bai, D.; Chen, Q.; Zhao, C. B.; Ren, T. H.; Huang, C. J.; North, M.; Xie, H. B. Facile preparation of polycarbonates from bio-based eugenol and 2-methoxy-4-vinylphenol. *Polym. Chem.* **2020**, *11*, 5133−5139.
(32) Boyd, D. A. Sulfur and its role in modern materials science. *Angew. Chem., Int. Ed.* **2016**, *55*, 15486−15502.
(33) Zhang, C. J.; Wu, H. L.; Li, Y.; Yang, J. L.; Zhang, X. H. Precise synthesis of sulfur-containing polymers via cooperative dual organocatalysts with high activity. *Nat. Commun.* **2018**, *9*, 2137.
(34) Gao, T. L.; Xia, X. C.; Tajima, K.; Yamamoto, T.; Isono, T.; Satoh, T. Polyether/polythioether synthesis via ring-opening polymerization of epoxides and episulfides catalyzed by alkali metal carboxylates. *Macromolecules* **2022**, *55*, 9373−9383.
(35) Stephan, J.; Stuhler, M. R.; Rupf, S. M.; Neale, S.; Plajer, A. J. Mechanistic mapping of (CS_2/CO_2)/epoxide copolymerization catalysis leads to terpolymers with improved degradability. *Cell Rep. Phys. Sci.* **2023**, *4*, No. 101510.
(36) Stühler, M. R.; Kreische, M.; Fornacon-Wood, C.; Rupf, S. M.; Langer, R.; Plajer, A. J. Monomer centred selectivity guidelines for sulfurated ring-opening copolymerisations. *Chem. Sci.* **2024**, *15*, 19029−19036.
(37) Gallizioli, C.; Battke, D.; Schlaad, H.; Deglmann, P.; Plajer, A. J. Ring-opening terpolymerisation of elemental sulfur waste with propylene oxide and carbon disulfide via lithium catalysis. *Angew. Chem., Int. Ed.* **2024**, *63*, No. e202319810.
(38) Quan, Y.; Ma, C. H.; Liu, Q. C.; Han, Z. Y.; Han, H. J.; Liao, X. J.; Sun, R. Y.; Xie, M. R. Green synthesis of well-defined linear poly(hydroxyl thioether) direct from epoxide in water. *Green Chem.* **2023**, *25*, 8082−8092.
(39) Sobczak, M.; Kędra, K. Biomedical polyurethanes for anticancer drug delivery systems: A brief, comprehensive review. *Int. J. Mol. Sci.* **2022**, *23*, 8181.
(40) Kuo, L.; Luijten, B. J.; Li, S.; de Moraes, A. C. M.; Silvaroli, A. J.; Wallace, S. G.; Hui, J.; Downing, J. R.; Shull, K. R.; Hersam, M. C. Sterilizable and reusable UV-resistant graphene-polyurethane elastomer composites. *ACS Appl. Mater. Interfaces* **2022**, *14*, 53241−53249.
(41) Dai, S.; Yue, S.; Ning, Z.; Jiang, N.; Gan, Z. Polydopamine nanoparticle-reinforced near-infrared light-triggered shape memory polycaprolactone-polydopamine polyurethane for biomedical implant applications. *ACS Appl. Mater. Interfaces* **2022**, *14*, 14668−14676.
(42) Zheng, N.; Fang, Z. Z.; Zou, W. K.; Zhao, Q.; Xie, T. Thermoset shape-memory polyurethane with intrinsic plasticity enabled by transcarbamoylation. *Angew. Chem., Int. Ed.* **2016**, *55*, 11421−11425.
(43) Elizalde, F.; Aguirresarobe, R. H.; Gonzalez, A.; Sardon, H. Dynamic polyurethane thermosets: tuning associative/dissociative behavior by catalyst selection. *Polym. Chem.* **2020**, *11*, 5386−5396.
(44) Wang, H.; Lin, W. S.; Qiu, X. Q.; Fu, F. B.; Zhong, R. S.; Liu, W. F.; Yang, D. J. In situ synthesis of flowerlike lignin/ZnO composite with excellent UV-absorption properties and its application in polyurethane. *ACS Sustain. Chem. Eng.* **2018**, *6*, 3696−3705.
(45) Zhou, Y. Y.; Tang, R. C. Natural flavonoid-functionalized silk fiber presenting antibacterial, antioxidant, and UV protection performance. *ACS Sustain. Chem. Eng.* **2017**, *5*, 10518−10526.
(46) Yue, P. P.; Rao, J.; Leng, Z. J.; Chen, G. G.; Hao, X.; Peng, P.; Peng, F. An electrospun composite of epoxidized *Eucommia ulmoides* gum and SiO_2-GO with ultraviolet resistance. *J. Mater. Sci.* **2022**, *57*, 4862−4875.
(47) Durairaj, A.; Maruthapandi, M.; Luong, J. H. T.; Perelshtein, I.; Gedanken, A. Enhanced UV protection, heavy metal detection, and antibacterial properties of biomass-derived carbon dots coated on protective fabrics. *ACS Appl. Bio Mater.* **2022**, *5*, 5790−5799.
(48) Hu, L. F.; Li, Y.; Liu, B.; Zhang, Y. Y.; Zhang, X. H. Alternating and regioregular copolymers with high refractive index from COS and biomass-derived epoxides. *RSC Adv.* **2017**, *7*, 49490−49497.

https://doi.org/10.1021/acs.macromol.5c00389
Macromolecules 2025, 58, 4769−4779